Bull. Chem. Soc. Jpn., 73, 1699—1713 (2000)

Accounts

Cause of the Memory Effect Observed in Alkaline Secondary Batteries Using Nickel Electrode

Yuichi Sato, * Shigeo Takeuchi, Shin'ichi Magaino,† and Koichi Kobayakawa

Departnent of Applied Chemistry, Faculty of Engineering, Kanagawa University, 3-27-1 Rokkakubashi, Kanagawa-ku, Yokohama 221-8686

†Kanagawa Industrial Technology Research Institute, 705-1 Shimoimaizumi, Ebina 243-0435

(Received March 31, 2000)

By repeating shallow discharging and overcharging of alkaline secondary batteries using nickel electrode, a lowering of working voltage is observed on the discharge curve, which is called a memory effect. The X-ray diffraction pattern of the charged-state of the normal nickel electrode contained only diffraction peaks due to β-NiOOH. A charged-state nickel electrode showing lowered discharge voltage had diffraction peaks due to γ-NiOOH in addition to those due to β-NiOOH. The formation of γ-NiOOH can be attributed to be the main cause for the memory effect commonly observed in alkaline secondary batteries such as nickel cadmium and nickel hydrogen batteries. By XRD analysis and AC impedance study, γ-NiOOH was found to be initially formed at the current collector side; it grows to the solution side in the course of shallow discharge-charge cycling. Therefore, if the amount of γ-NiOOH formed is small, only β-NiOOH can be detected, even when the memory effect is observed. In this case, γ-NiOOH can be detected by shaving the surface of the electrode using a piece of emery paper to remove covering β-NiOOH. This γ-NiOOH disappears within a few cycles of the normal charge-discharge cycling, resulting in the elimination of the memory effect. It may be concluded that the cause of the memory effect is mainly due to the formation of γ-NiOOH.

Rechargeable alkaline Ni-based batteries, such as nickel-cadmium (Ni/Cd), nickel-hydrogen (Ni/H_2) and nickel-hydrogen battery with a metal hydride negative electrode (Ni/MH, where M means hydrogen absorbing alloys) are widely used in today's space and portable applications, the latter being very promising for electric vehicles.

The memory effect frequently coming across in these alkaline secondary batteries can be described as an apparent reduction in cell capacity to a predetermined cutoff voltage resulting from highly repetitive patterns of use. If a battery has been cycled to a certain depth of discharge for a large number of cycles for instance, the battery will not produce a greater capacity than that corresponding to the applied cycling regime in a subsequent normal discharge.

At first, this phenomenon was observed in Ni/Cd batteries and the cell failures was believed to involve penetration of cadmium plate material through the separator.[1] Reconditioning has traditionally been utilized as a tool for maintaining the performance of normal cells and batteries, where the cells or batteries are enforced to discharge to make the capacity empty. During the reconditioning, the deep discharge causes to decrease the electrode conductivity to a low value and the shorting tendency is reduced or eliminated, although not permanently. Thus it has been understood that the application of reconditioning produces a net reduction of conductivity at shorting sites. There is another presumption that it is related mainly to a physical change in the negative electrode which is due to the formation of intermetallic compounds of cadmium and the sintered nickel support.[2] If this is true, a Ni/H_2 battery where the negative electrode is comprised of a metal hydride having no cadmium does not have the memory effect.[3,4] However, the memory effect has been also observed in Ni/MH batteries.[5,6] Takeno et al. concluded that the memory effect was associated with lowered discharge voltage in the nickel positive electrode,[5] although they showed no detailed mechanism. Kuwajima et al. also observed the memory effect in a Ni/H_2 batteries for use in space.[7] Therefore, it may be concluded that the cause of the memory effect is mainly in the nickel electrode. Recently, Ni–MH batteries have gained much attention as a most promising candidate for the power sources of hybrid cars (HEV) and EV.[6] It is therefore interesting and worthwhile to clarify the cause of the memory effect. In this paper, we report that the cause of the memory effect observed in alkaline secondary batteries using nickel electrode appears to be present in the nickel electrode.

1. Demonstration of the Memory Effect

Figure 1 shows the discharge curves of various states of a sintered-type commercial AAA Ni/Cd battery with a nominal capacity of 250 mA h (height: 43 mm, diameter: 9.1 mm), where curve A is the normal discharge curve and curve B reveals the memory effect. To obtain curve B, the following charge-discharge cycling was conducted. At first, three normal charge-discharge cycles were conducted for the AAA size battery, where charging was conducted at a constant current of 25 mA for 16 h and discharging at a constant current of 250 mA to a 0.8 V cutoff voltage. Then, 50 charge-discharge cycles were conducted at a charging current of 25 mA for 10 h and a discharging current of 50 mA to a 1.20 V cutoff voltage. Afterwards, the diagnostic test of normal discharge was conducted at a constant current of 250 mA h to an 0.8 V cutoff voltage, resulting curve being curve B. When we repeat one or two cycles of normal charge-discharge cycling, the memory effect was removed considerably (curves C and D in Fig. 1).

For Ni/MH batteries, the memory effect is also observed as seen in Fig. 2 as discharge curve B. In this case, a paste-type AAA (height: 43 mm, diameter: 9.1 mm) commercial nickel-hydrogen secondary battery with a nominal capacity of 550 mA h was used for demonstrating the memory effect. For the AAA nickel-hydrogen battery, five normal charge-discharge cycles were conducted, where charging was conducted at a constant current of 50 mA for 16 h and a discharging current of 250 mA to a 0.8 V cutoff voltage. Then, 300 charge-discharge cycles were conducted at a charging current of 50 mA for 16 h and a discharging current of 50 mA to a 1.20 V cutoff voltage. After repeating this shallow discharging and overcharging, normal discharge was conducted at a constant current of 250 mA to a 0.8 V (curve B).

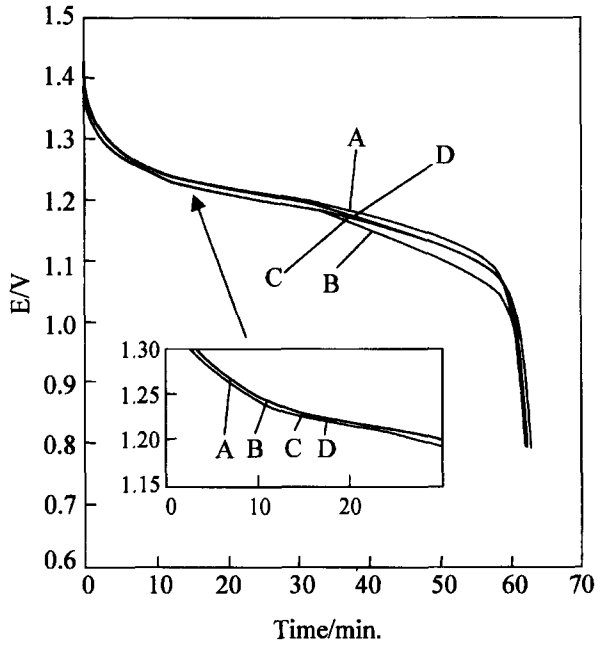

Fig. 1. Discharge curves of AAA size nickel–cadmium battery at 250 mA and at 30 °C. (A) Discharge curve of normal-state cell; (B) first discharge curve; (C) second discharge curve; (D) third discharge curve after 50 cycles charge-discharge cycling. Charging was carried out at 25 mA for 16 h in curves A to D.

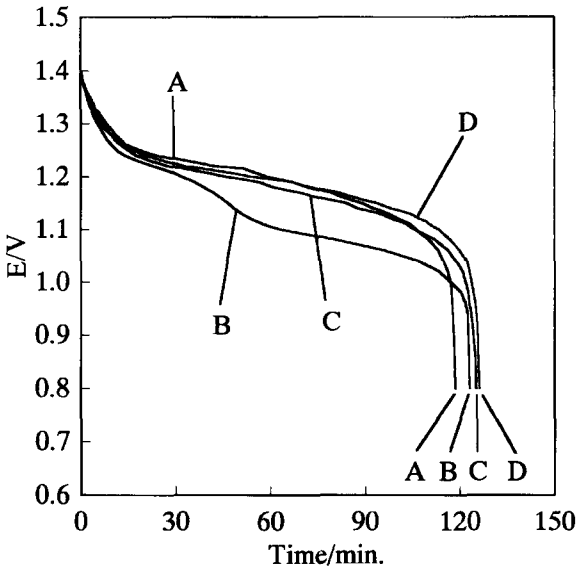

Fig. 2. Discharge curves of AAA size nickel–hydrogen battery at 250 mA and at 30 °C (A) Discharge curve of normal-state cell; (B) first discharge curve; (C) second discharge curve; (D) third discharge curve after 300 cycles charge–discharge cycling. Charging was carried out at 50 mA for 16 h in curves A to D.

2. Survey of the Cause of the Memory Effect[8]

2.1 Construction of the Small Size Cells and the Memory Effect Causing Charge-Discharge Mode. To produce the memory effect in commercial batteries such as a AAA size battery, it takes a long time as stated above. Therefore, we made small size cells to cause the memory effect in a short time. Nickel and cadmium electrodes were taken from a sintered-type commercial AAA Ni/Cd battery. We fabricated two different types of cells, i.e., the one is the positive (nickel) electrode capacity-limited and the other, the negative (cadmium) electrode capacity-limited. The nickel capacity-limited cell was fabricated from a 1.5 cm×1.5 cm nickel sheet electrode cut from the electrode of a AAA size battery, then wrapped with a polypropylene non-woven fabric separator. It was placed between two sheets of a 3 cm×3 cm cadmium electrode having sufficiently a greater capacity than that of the nickel electrode. These electrodes were then sandwiched between two many-holed thin acrylic resin plates, and the assembly was tightly bolted at the four corners. The cell construction was reversed for the cadmium capacity-limited cell. These cells had a capacity of about 60 mA h. Charge-discharge cycling was conducted in an 8 M KOH solution (1 M = 1 mol dm^{-3}) at 30±1 °C (Fig. 3) using a charge-discharge unit (Hokuto Denko Co., 6ch HJ101MS) and a Y–T recorder (Yokogawa Electric Corp., micro R180, model 4176) or a charge-discharge unit (Toyo System Co., TYS-30TUOO) with a personal computer (PC) and charge-

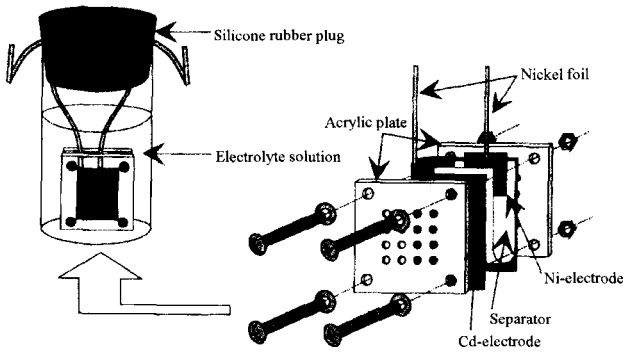

Fig. 3. Cell construction for nickel capacity-limited cell.

discharge controlling software.

Three normal charge-discharge cycles were conducted at 10 mA (2.22 mA cm^{-2}) of charging current for 7 h and 20 mA (4.44 mA cm^{-2}) of discharging current to an 0.8 V cutoff voltage for small nickel and cadmium capacity-limited cells. The nickel and cadmium capacity-limited cells show good cyclability. The memory effect was then brought about by cycling at 10 mA (2.22 mA cm^{-2}) of charging current for 7 h and at 10 mA (2.22 mA cm^{-2}) of discharging current to a 1.2 V cutoff voltage after repeating 50 charge-discharge cycles under these conditions, which is called the memory effect causing charge-discharge cycling. Then, as a diagonostic discharge, the cell was discharged in the normal discharge mode of 20 mA to an 0.8 V cutoff voltage. Using these cells, the memory effect was produced by a charge-discharge cycling test to clarify the cause of the memory effect.

2.2 Charge-Discharge Behavior of the Small Size Cells. Figure 4 shows results for the nickel capacity-limited cell. Curve A is the normal discharge curve and curve B the first discharge curve after 50 cycles of the memory effect producing charge-discharge cycling, where voltage lowering was clearly observed. Before obtaining curve B, the cadmium electrode was replaced by a new one in a charged state whose capacity was larger than that of the nickel electrode, because the cadmium electrode may have been affected by the preceding 50-cycle charge-discharge regime causing the memory effect. Therefore, the cadmium electrode was replaced by a new one to observe only nickel electrode behavior after 50-cycle, and the diagnostic discharging was conducted. However, the discharge curve of the cell without replacement showed almost the same shape as curve B (Fig. 4). It should be noted that the discharge time was prolonged by about 40% for curve B compared to normal discharge curve A, although the discharge voltage was lower than that of a normal discharge curve. Curve C was obtained after measuring curve B and charging at 10 mA for 7 h. As seen from curve C, voltage lowering disappeared easily and discharge curve almost recovered the normal state. There may be some doubt as to whether discharge curve B in Fig. 4 exhibits the classic memory effect phenomenon observed in nickel cadmium batteries in practical use (curve B in Fig. 1). We think the phenomenon observed in our experimental small cells is the same as the memory effect observed in practical nickel

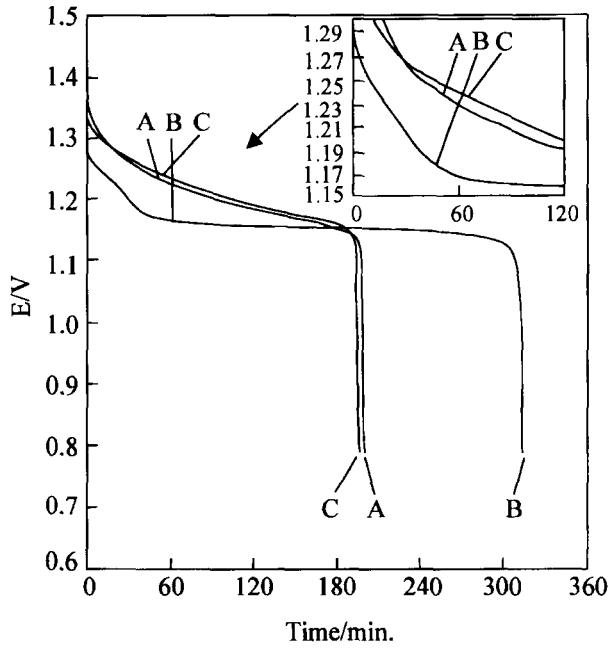

Fig. 4. Discharge curves of nickel capacity-limited cell at 4.44 mA cm^{-2} and at 30 °C. (A) Discharge curve of normal-state cell; (B) first discharge curve; (C) second discharge curve after 50 cycles charge–discharge cycling. Charging was carried out at 2.22 mA cm^{-2} for 7 h in curves A to C.

cadmium batteries, because nearly the same shape discharge curve is also obtained in our small size nickel limited cells when the number of the shallow charge-discharge cycling is small (vide Fig. 11, curve B). At any rate, we investigated the reason why the working voltage lowering occurs at the first discharge curve after 50 cycles of charge-discharge cycling (curve B in Fig. 4).

The discharge voltage of curve B in the cadmium capacity-limited nickel–cadmium cell, which is the first discharge curve after 50 cycles of the charge-discharge regime causing the memory effect (Fig. 5), is about 40 mV lower than that of the normal cell (curve A), where the nickel electrode was replaced with a new charged-state electrode to observe only cadmium electrode behavior after 50-cycle charge-discharge cycling. The degree to which voltage was lowered, however, is greater in the nickel capacity-limited cell, as is shown by comparing curve B in Fig. 4 with curve B in Fig. 5. Curves B and C in Fig. 5 are the second and third discharge curves after 50-cycle charge-discharge cycling. The discharge voltage had recovered somewhat, but the phenomenon seems somewhat different from that in the nickel capacity-limited cell (curves C and D in Fig. 4). With the nickel capacity-limited cell, the discharge curve recovered at once to the normal shape in only one or two cycles of deep discharging to 0.8 V and charging. The cause of the lowered voltage for curve B in Figs. 4 and 5 may thus differ, as is discussed later. The charged-state nickel and cadmium electrode potentials before and after the voltage lowering obtained from the nickel and cadmium capacity-limited cells, were measured vs. an Hg/HgO(KOH) electrode (Fig. 6). The nickel electrode po-

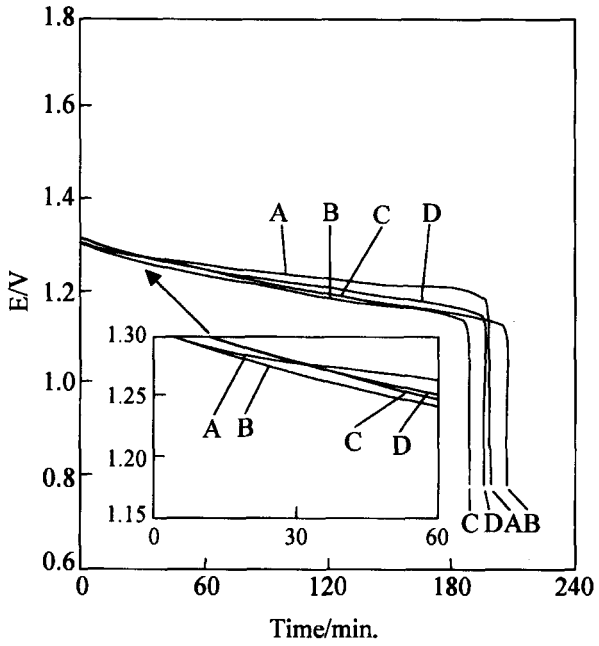

Fig. 5. Discharge curves of cadmium capacity-limited cell at 4.44 mA cm^{-2} and at 30 °C. (A) Discharge curve of normal-state cell; (B) first discharge curve; (C) second discharge curve; (D) third discharge curve after 50 cycles charge–discharge cycling. Charging was carried out at 2.22 mA cm^{-2} for 7 h in curves A to D.

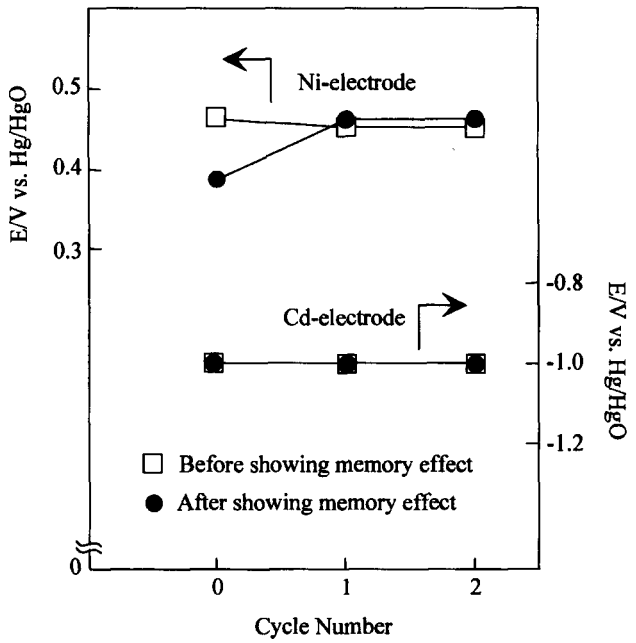

Fig. 6. Charged-state nickel and cadmium electrode potentials change in normal charge–discharge cycling before (□) and after (●) showing voltage lowering.

tential of the charged state just after the 50 cycle memory effect producing charge-discharge cycling (corresponding to cycle number zero) is about 75 mV lower than that of the normal-state nickel electrode, but it recovered to the normal value after one cycle of discharging to 0.8 V and charging. In contrast, charged-state cadmium electrode potentials were almost the same before and after 50 cycle charge-discharge cycling producing the memory effect. These results suggest that voltage lowering in the nickel capacity-limited cell after the memory effect producing charge-discharge cycling is mainly due to the nickel electrode rather than to the cadmium electrode.

2.3 XRD Analysis and SEM Observation of the Electrode Surface. X-Ray diffraction analysis was conducted for a nickel electrode in the charged (Fig. 7) and discharged (Fig. 8) states, using a Geigerflex RAD-gA (Rigaku Co., Cu $K\alpha$, 40 kV, 100 mA). A comparison of diffraction patterns A and B with C in Fig. 7 showed that diffraction peaks due to γ-NiOOH are observed in C, which is the diffraction pattern of the charged-state electrode after the 50-cycle memory effect producing charge-discharge cycling. If this electrode is discharged to 0.8 V or is overdischarged, the diffraction peak due to γ-NiOOH disappeared (diffraction patterns C and E in Fig. 8), but it is observed if the depth of discharge is shallow (D in Fig. 8). These results indicate

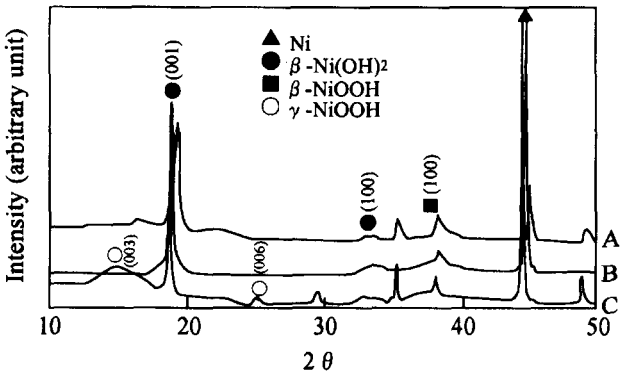

Fig. 7. XRD patterns for charged-state nickel electrode. (A) Normal electrode; (B) normal electrode after overcharging at 2.22 mA cm^{-2} for 24 h; (C) electrode after 50-cycles charge–discharge cycling.

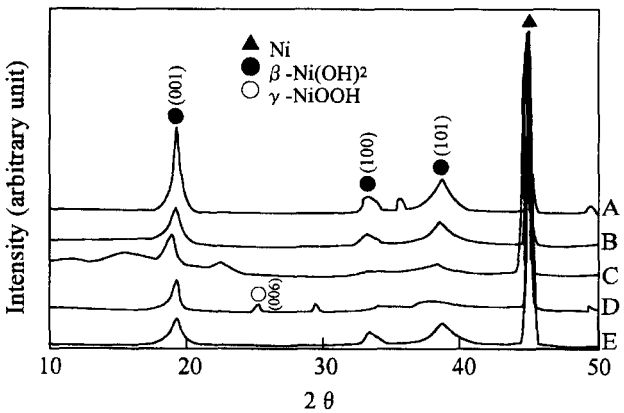

Fig. 8. XRD patterns for discharged-state nickel electrode. (A) Normal electrode; (B) normal electrode after overdischarging at 2.22 mA cm^{-2} for 24 h; (C) electrode discharged to 0.8 V at 2.22 mA cm^{-2} after 50 cycles charge–discharge cycling; (D) electrode discharged to 1.2 V at 2.22 mA cm^{-2} after 50 cycles charge–discharge cycling; (E) electrode overdischarged at 2.22 mA cm^{-2} for 24 h after 50 cycles charge–discharge cycling.

that the electrode showing voltage lowering in the charged state contains γ-NiOOH, which disappears on one deep discharge such as the discharge to 0.8 V. The origin of the diffraction peaks observed at about 29.5° and 36° and 49° is not clear, but may be due to additives such as cobalt, or cadmium, probably $Cd(OH)_2$ used to enhance the nickel electrode performance.[9—12]

It is said that β-nickel hydroxide is converted to γ-NiOOH on prolonged charging irreversibly damaging the electrode due to accompanying mechanical deformation.[13] The discharge of a nickel electrode containing γ-NiOOH proceeds at more negative potentials than that of a nickel electrode having β-NiOOH as the active material.[14,15] This is related to the different electrochemical potentials of these phases.[16] The discharge capacity is, as a rule, higher for electrodes containing γ-NiOOH,[14] which is caused by a higher nickel oxidation state; in γ-NiOOH, it can reach values close to 3.7, while in β-NiOOH, it only slightly exceeds 3.2.[16] Our experimental results and assumption that the voltage is lowered due to γ-NiOOH formed by 50-cycles of shallow discharge and overcharge are not inconsistent with the above description for γ-NiOOH. The lower discharge voltage but higher capacity of the nickel capacity-limited cell (Fig. 4, curve B) is thus understandable, if it is due to γ-NiOOH formed on the nickel electrode by the memory effect causing charge-discharge cycling.

The surfaces of both nickel and cadmium electrodes were observed with a scanning electron microscope (SEM) (Elionix Co., ELS-3300). SEM photographs of charged-state nickel and cadmium electrodes (Figs. 9 and 10) indicate that the shape of the charged-state nickel oxide showing voltage lowering (B in Fig. 9) differs from that produced by normal charge–discharge cycling (A), i.e., the particle size of the nickel oxide expands, and grows like a stiff string. In contrast, the surface of the normal-state nickel electrode (A) shows a relatively flat surface with sporadic cracks. On the surface of the cadmium electrode after 50 charge–discharge cycles causing the memory effect, pyramidal crystals occur (B in Fig. 10). The pyramidal crystals seems decrease the actual electrode surface area. The actual discharge current density will therefore increase and the iR drop also increases, which decreases the working voltage of the cadmium electrode (curves B in Fig. 5). In such a case, the second and third discharge curves (curves C and D in Fig. 5) would not recover to the normal discharge curve (curve A), because the pyramidal crystal (B in Fig. 10) could not be changed easily to the initial state by only one or two cycles of normal charge–discharge cycling.

From all these results and discussion, we concluded that voltage lowering, i.e., the memory effect, is due to the nickel electrode, and γ-NiOOH formation appears to cause the memory effect, although the mechanism is not so simple in practical batteries.

3. Reaffirmation of the Cause of the Memory Effect

When we reported that the memory effect occurred because β-NiOOH changed to γ-NiOOH by over-charging

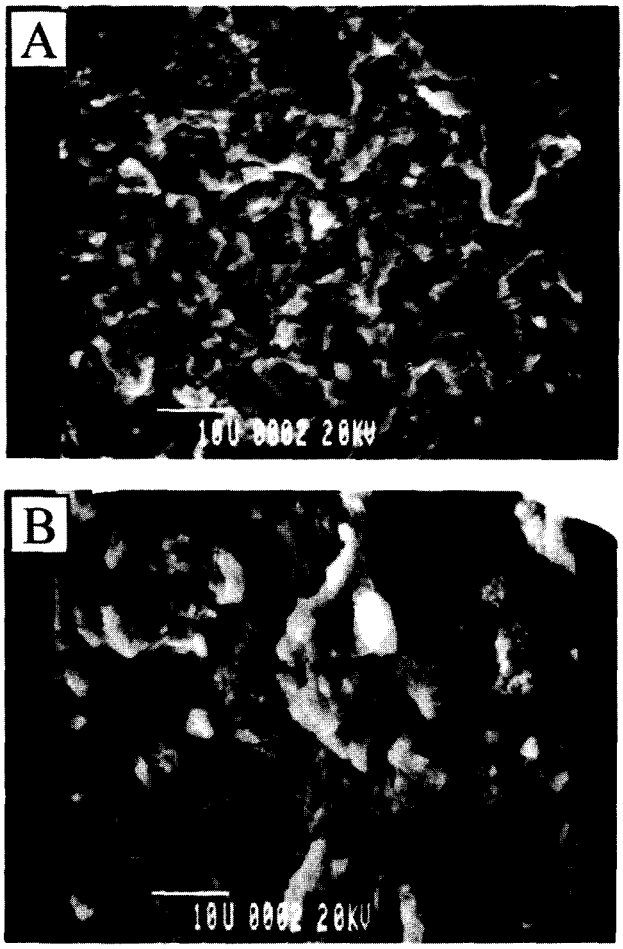

Fig. 9. SEM photographs of nickel electrode surface. (A) Charged-state electrode after 20 cycles of normal charge–discharge cycling; (B) charged-state electrode after 50 cycles charge–discharge cycling.

in a previous paper[8] or at academic meetings, there was a counterargument that the memory effect occurred even when γ-NiOOH could not be observe.[17] Therefore, we further studied to clarify the cause of the memory effect and concluded that it occurs due to the formation of γ-NiOOH. Although the formation of γ-NiOOH has been frequently studied[18—20] and some additives such as cobalt, cadmium, $Ca(OH)_2$ and $Zn(OH)_2$ to prevent the formation of γ-NiOOH have been presented[21—25], few of the studies appear to have noticed that the formation of γ-NiOOH is the cause of memory effect except present authors.[8] In this section, we reaffirm that the memory effect occurs due to the formation of γ-NiOOH.

3.1 Discharge Curves after Shallow Discharge–Charge Cycling and XRD Analysis of the Nickel Electrode.[26] This time, a small sized nickel capacity-limited cell with a capacity of about 75 mA h was fabricated using a 1.8×1.8 cm nickel sheet electrode cut from the sintered-type nickel electrode of a commercial AAA battery and two sheets of 3.3×3.5 cm cadmium electrode with a greater capacity, of which capacity was about 3.6 times larger than that of the nickel electrode.

At first, five normal charge-discharge cycles were con-

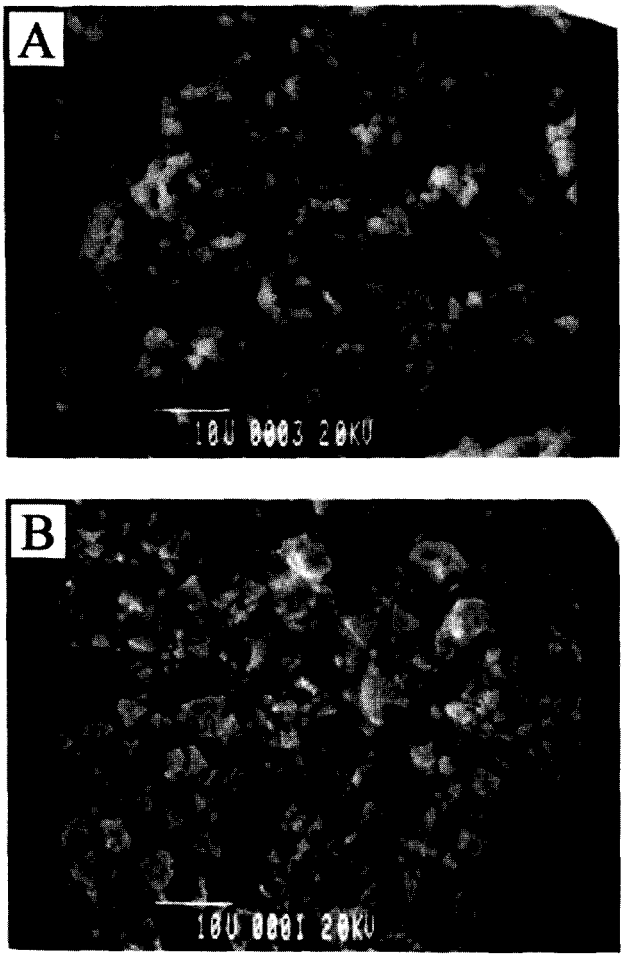

Fig. 10. SEM photographs of cadmium electrode surface. (A) Charged-state electrode after 20 cycles of normal charge–discharge cycling; (B) charged-state electrode after 50 cycles charge–discharge cycling.

ducted for a nickel capacity-limited cell, where charging was conducted at a constant current of 20 mA (3.2 mA cm^{-2}) of charging current for 5 h and 20 mA (3.2 mA cm^{-2}) of discharging current to an 0.8 V cutoff voltage. Then, cycling at 20 mA (3.2 mA cm^{-2}) of charging current for 5 h and at 20 mA (3.2 mA cm^{-2}) of discharging current to a 1.2 V cutoff voltage was conducted for appropriate cycles to produce a memory effect (shallow discharge–charge cycling). After repeating appropriate charge–discharge cycles under these conditions, the cell was discharged at the normal discharge rate of 20 mA (3.2 mA cm^{-2}) to an 0.8 V cutoff voltage to see the effect of the preceding shallow discharge–charge cycles and then charged for 5 h at 3.2 mA cm^{-2} to obtain the second discharge curve. Figure 11 shows the discharge curves of the small size nickel capacity-limited nickel–cadmium cell. Curve A is the normal discharge curve. Curve B is the first discharge curve for the cell after 5-cycles shallow discharge–charge cycling. As seen in the enlarged figure, clearly the working voltage of curve B is lowered, i.e. a memory effect appeared, and this voltage lowering recovered to a normal discharge curve after the next normal charge–discharge cycling as seen in curves C and D. X-Ray

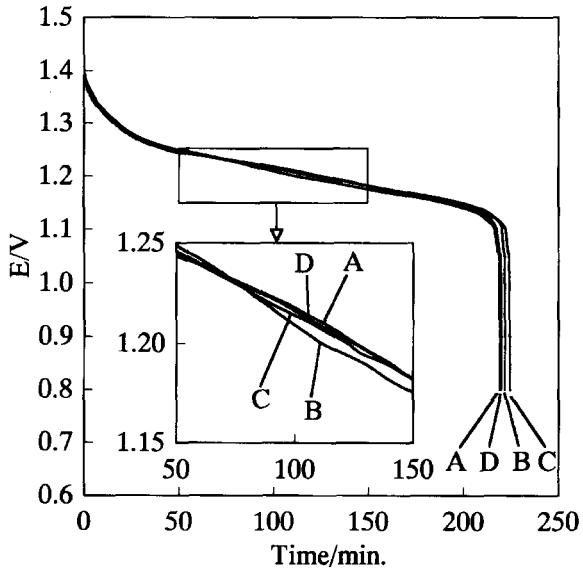

Fig. 11. Discharge curves of nickel capacity-limited cell at 3.2 mA cm^{-2} and at 30 °C. (A) Discharge curve of normal-state cell; (B) first discharge curve; (C) second discharge curve; (D) third discharge curve after 5 cycles shallow discharge–charge cycling. Charging was carried out at 3.2 mA cm^{-2} for 5 h in curves A to D.

diffraction analysis was conducted for a charged state nickel electrode obtained by normal charge–discharge cycling and that obtained by 5-cycles shallow discharge–charge cycling. These XRD patterns are shown in Fig. 12. The diffraction pattern of charged state normal electrode A and electrode B, which is the charged-state electrode after 5-cycles shallow charge–discharge cycling, did not exhibit the diffraction

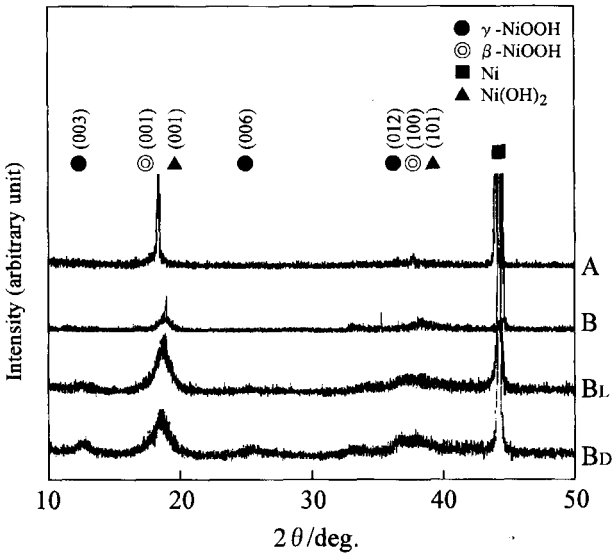

Fig. 12. XRD patterns for charged-state nickel electrode. (A) Normal electrode; (B) electrode after 5 cycles shallow discharge–charge cycling; (B_L) 0.11 mm shaved electrode (electrode thinckness: 0.12 mm) after 5 cycles shallow discharge–charge cycling; (B_D) 0.17 mm shaved electrode (electrode thickness: 0.06 mm) after 5 cycles shallow discharge–charge cycling.

peaks due to γ-NiOOH. However, after shaving the surface of this 5-cycled electrode B using a piece of emery paper, diffraction peaks due to γ-NiOOH clearly appeared at about 13 and 26 degrees of diffraction angle as seen in B_L (lightly shaved) and B_D (deeply shaved). On the other hand, 0.17 mm shaved electrode after normal charge–discharge cycling showed no peaks corresponding to γ-NiOOH, though its XRD pattern is not shown here. This observation suggests that γ-NiOOH is present in the inside of the electrode. For the discharged-state electrode after measuring curve B in Fig. 11, and charged-state electrodes after measuring curve B (i.e., the electrode before measuring curve C in Fig. 11) and C (the electrode before measuring curve D in Fig. 11), diffraction peaks due to γ-NiOOH could not be observed even in the shaved state. Therefore, γ-NiOOH observed in electrode B in Fig. 12 disappeared by normal discharging to 0.8 V. For the charged-state shaved electrode after repeating normal charge–discharge cycling, NiOOH could not be observed. Increasing the cycle numbers of shallow discharge–charge cycling, the working voltage lowering became more pronounced as seen in Fig. 13, curve B compared to curve B in Fig. 11. After 100 cycles of charge–discharge shallow cycling, the discharge curve showing low voltage did not easily recover to the normal curve as shown in curves C and D. The voltage difference observed in the initial parts of curves A, B, C, and D seems to depend on the quantity of γ-NiOOH left in the interface between substrate and active materials. In the charged state of the 100 charge–discharge cycling electrode, a very small diffraction peak due to γ-NiOOH at about 13 degree appeared as shown in diffraction pattern B in Fig. 14. After shaving this electrode, diffraction peaks due to γ-NiOOH became clearer as seen in the diffraction patterns of B_L and B_D. For the charged state electrode obtained after measuring the discharging curve D in Fig. 13,

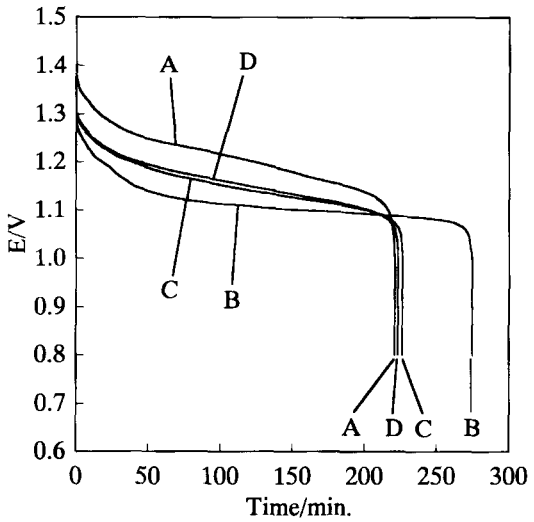

Fig. 13. Discharge curves of nickel capacity-limited cell at 3.2 mA cm^{-2} and at 30 °C. (A) Discharge curve of normal-state cell; (B) first discharge curve; (C) second discharge curve; (D) third discharge curve after 100 cycles shallow discharge-charge cycling; charging was carried out at 3.2 mA cm^{-2} for 5 h in curves A to D.

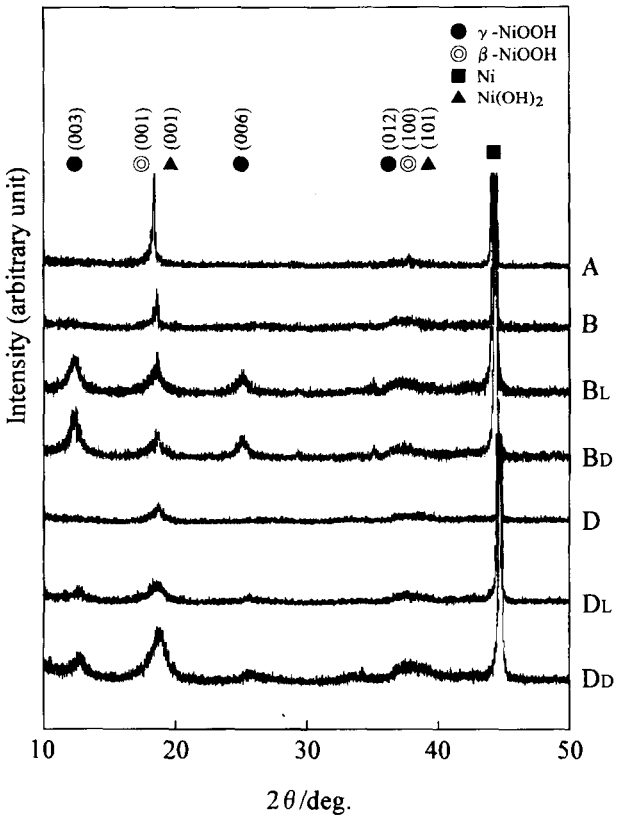

Fig. 14. XRD patterns for (A) charged-state normal nickel electrode; (B) charged-state electrode after 100 cycles shallow discharge–charge cycling; (B_L) 0.10 mm shaved electrode (electrode thickness: 0.13 mm) of electrode B; (B_D) 0.20 mm shaved electrode (electrode thickness: 0.04 mm) of electrode B; (D) charged-state electrode after measuring curve D in Fig. 13; (D_L) 0.10 mm shaved electrode (electrode thickness: 0.13 mm) of electrode D; (D_D) 0.17 mm shaved electrode (electrode thickness: 0.06 mm) of electrode D.

XRD analysis was conducted (Fig. 14). In this case, smaller diffraction peaks due to γ-NiOOH compared to that of B_L and B_D were observed for the shaved electrodes (D_L and D_D). This means that the amount of γ-NiOOH decreased by 2 or 3 cycles of normal discharging, but remained in the electrode showing the voltage lowering phenomena as seen in curve D in Fig. 13. It is well known that the discharge potential of γ-NiOOH is lower than that of β-NiOOH and the discharge capacity is, as a rule, larger for γ-NiOOH than for β-NiOOH, which is caused by a higher oxidation state of γ-NiOOH.[14–16,27] Our experimental results are not inconsistent with these descriptions for γ-NiOOH.

Shallow discharge–charge cycling seems to correspond to overcharging. Therefore, using commercial AAA size nickel-cadmium battery, 1000 h of overcharging at 50 mA of charging current was carried out. As seen in curve B of Fig. 15, clearly voltage lowering and prolonged discharge time were observed as seen in curve B of Fig. 13. This overcharged state shaved electrode also showed the presence of γ-NiOOH as seen for shaved electrodes B_L and B_D in Fig. 16. All these results cited above are for Ni/Cd batteries. Then,

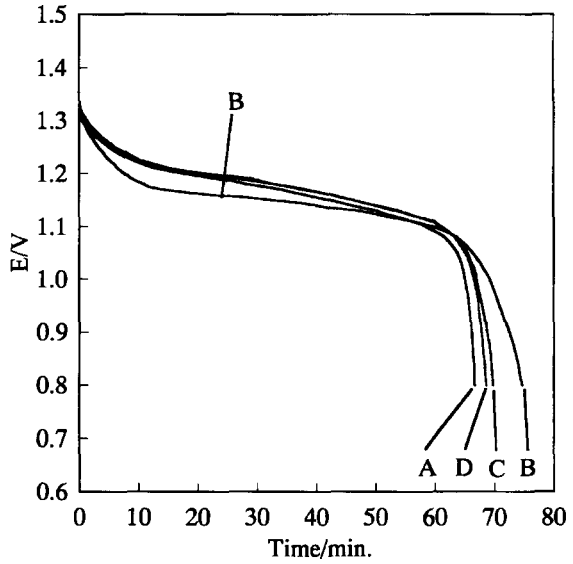

Fig. 15. Discharge curves of AAA size nickel-cadmium battery at 250 mA and at 30 °C. (A) Discharge curve of normal-state cell; (B) first discharge curve; (C) second discharge curve; (D) third discharge curve after 1000 h overcharging at 50 mA. Charging was carried out at 50 mA for 7 h in curves A to D.

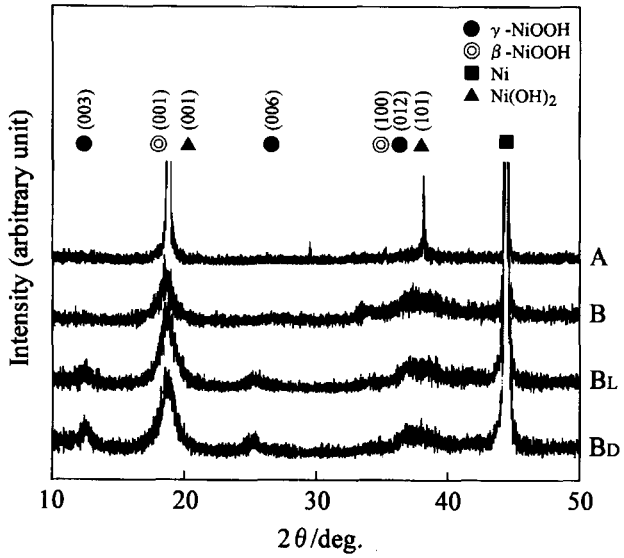

Fig. 16. XRD patterns for charged-state nickel electrode obtained from AAA size nickel-cadmium battery. (A) Normal electrode; (B) electrode after 1000 h overcharging at 50 mA; (B_L) 0.10 mm shaved electrode (electrode thickness: 0.13 mm) of electrode B; (B_D) 0.19 mm shaved electrode (electrode thickness: 0.03 mm) of electrode B.

commercial AAA size Ni/MH battery was also tested, i.e. 5000 h overcharging was carried out; the discharge curves are shown in Fig. 17. For 300 cycles shallow discharge-charge cycling of Ni/MH, their discharge curves were already shown in Fig. 2. Curve B in Fig. 17 is the first discharge curve of the 5000 h overcharging one, where the working voltage is lowered and discharging time is prolonged, i.e. a memory effect was also observed in nickel-hydrogen battery. Second

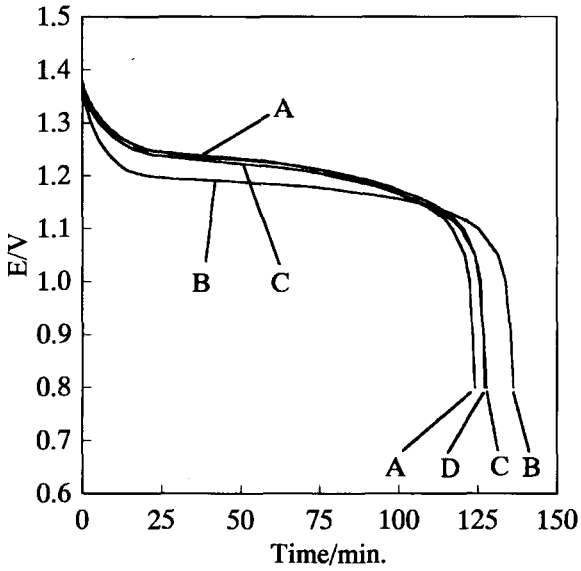

Fig. 17. Discharge curves of AAA size nickel-hydrogen battery at 250 mA and at 30 °C. (A) Discharge curve of normal-state cell: (B) first discharge curve; (C) second discharge curve; (D) third discharge curve after 5000 h overcharging at 50 mA. Charging was carried out at 50 mA for 7 h in curves A to D.

(Curve C) and third (curve D) discharge curves recovered almost to the normal discharge curve A. XRD analysis for the charged state nickel electrode after 300 cycles charge–discharge cycling was conducted. NiOOH powder obtained from this electrode showed a small diffraction peak due to γ-NiOOH at about 13 degrees (Fig. 18, B_P). As this electrode is a paste type made by impregnating nickel fiber substrate with nickel hydroxide, shaved state can not be obtained like a sintered type nickel electrode of nickel-cadmium battery. For the NiOOH powder of 5000 h overcharged battery, almost

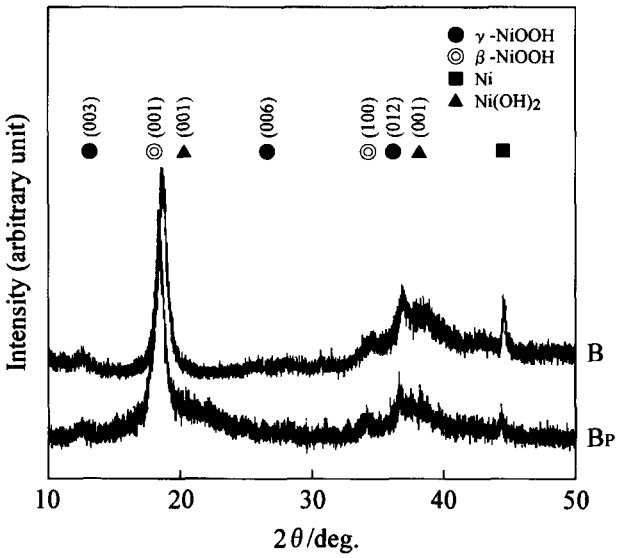

Fig. 18. XRD patterns for charged-state nickel electrode obtained from AAA size nickel-hydrogen battery. (B) Electrode after 300 cycles charge–discharge cycling; (B_P) nickel oxide powder obtained from electrode B.

the same XRD pattern as B_P in Fig. 18 was obtained. The reason why the shape of diffraction patterns between NiOOH of nickel–cadmium and nickel–hydrogen is different seems mainly due to the batteries being products of different battery makers, i.e. different materials may be added.

From previous results and discussion, it may be concluded that γ-NiOOH cannot be detected for the charged state Ni electrode on conducting some cycles of shallow discharge–charge cycling, if its amount is small and the X-rays cannot reach the γ-NiOOH phase. In this case, if the surface of the Ni electrode is shaved and surface β-NiOOH is removed, γ-NiOOH can be detected (Fig. 19). Therefore, we assume that β-NiOOH is formed under the normal charging conditions; however, γ-NiOOH will be initially formed at the collector side and grow to the solution side under the overcharging conditions such as repetitive shallow discharge–charge cycling.

3.2 Estimation of the γ-NiOOH Formation Mechanism by A. C. Impedance Study.[28] From the above results and discussion, it is found that γ-NiOOH begins to form at the interface between the substrate and $Ni(OH)_2$ active materials and it grows to the solution side. In order to observe the resistance change in the Ni electrode with shallow charge–discharge cycling, A. C. impedance was measured for Ni electrodes in various charged states by adding ± 5 mV between 10 kHz—1 mHz. Figure 20 shows the Cole–Cole plots for various charge states of Ni electrodes after cycling from 5 to 20 cycles, where the semicircle is due to the charge transfer resistance and the line at 45° is due to diffusion. On plotting the resistances obtained from the diameter of the impedance loop at the higher frequency side vs. cycle number, the resistance is found to increase with the cycle number (Fig. 21).

In order to understand this phenomenon, we estimate the reaction process at the Ni electrode as in Fig. 22. In the charging process, a hydroxide ion in aqueous solution reacts with a proton which diffuses in the nickel hydroxide crystal to produces a water molecule, and Ni(II) is oxidized to Ni(III) to produce β-NiOOH. On further charging, β-NiOOH is changed to γ-NiOOH. The following reaction sequence has been chosen to describe the charging processes:

$$\{Ni(OH)_2\}_{ads} \underset{k_{1c}}{\overset{k_{1a}}{\rightleftharpoons}} (NiOOH)_{ads} + H_m^+ + e^- \quad (1)$$

$$(NiOOH)_{ads} + \{Ni(OH)_2\}_{bulk} \underset{k_{eb}}{\overset{k_{ef}}{\rightleftharpoons}} (NiOOH)_{bulk} + \{Ni(OH)_2\}_{ads} \quad (2)$$

$$\left[\begin{array}{l} \{Ni(OH)_2\}_{bulk} \rightleftharpoons (NiOOH)_{bulk} + H_b^+ + e^- \\ H_b^+ \overset{\text{diffusion}}{\rightleftharpoons} H_m^+ \\ (NiOOH)_{ads} + H_m^+ + e^- \rightleftharpoons \{Ni(OH)_2\}_{ads} \end{array}\right] \quad (2')$$

$$H_m^+ \overset{\text{diffusion}}{\rightleftharpoons} H_s^+ \quad (3)$$

$$H_s^+ + OH^- \underset{k_{hc}}{\overset{k_{ha}}{\rightleftharpoons}} H_2O \quad (4)$$

In Eqs. 1 and 2, k with a subscript means a reaction rate constant.

At first, nickel hydroxide [$\{Ni(OH)_2\}_{ads}$] present near the collector is oxidized to nickel hydroxide oxide $\{(NiOOH)_{ads}\}$ in the charging process (Eq. 1), but it acquires a proton (H_b^+) and a electron from the bulk nickel hydroxide [$\{Ni(OH)_2\}_{bulk}$] to revert to nickel hydroxide [$\{Ni(OH)_2\}_{ads}$]. Bulk nickel hydroxide [$\{Ni(OH)_2\}_{bulk}$] deprived of a proton and an electron is oxidized to nickel hydroxide oxide $\{(NiOOH)_{bulk}\}$. By repeating this process, nickel hydroxide oxide is formed sequentially in the bulk nickel hydroxide. These processes written in Eq. 2′ are summarized in Eq. 2. Equation 3 shows that a proton present at the interface between the collector and the active material (H_m^+) diffuses to the interface between the active material and the solution. Equation 4 shows that a proton present at the interface between the active material and the solution (H_s^+) reacts with OH^- in the solution to produce a water molecule. In the discharging process, the reverse reactions are assumed to occur.

Reaction rates are assigned as r_{1a}, r_{ef}, r_{ha} for Eqs. 1, 2, and 4, the reverse reaction rates as r_{1c}, r_{eb}, r_{hc}, and the diffusion rate for Eq. 3 as r_d. If reaction rates are expressed as the product of the proportional constant and concentrations for simplicity, the reaction rates can be represented as Eqs. 5, 6, 7, 8, 9, 10, and 11.

$$r_{1a} = k_{1a}\theta \quad (5)$$

$$r_{1c} = k_{1c}(1-\theta)c_{Hm} \quad (6)$$

$$r_{ef} = k_{ef}(1-\theta)c_{NH} \quad (7)$$

$$r_{eb} = k_{eb}\theta c_{NO} \quad (8)$$

$$r_d = D\frac{c_{Hm} - c_{Hs}}{\delta} \quad (9)$$

$$r_{ha} = k_{ha}c_{Hs}c_{OH} \quad (10)$$

$$r_{hc} = k_{hc} \quad (11)$$

where θ denotes the surface coverage of nickel hydroxide [$\{Ni(OH)_2\}_{ads}$] on the collector, c_{Hm} the proton concentration (H_m^+) at the interface between collector/solution, c_{NH} the bulk nickel hydroxide concentration [$\{Ni(OH)_2\}_{bulk}$] in the active materials, c_{NO} the bulk nickel hydroxide oxide concentration [$(NiOOH)_{bulk}$] in the active materials, c_{HS} the proton concentration at the interface between the active material and the solution, D the diffusion coefficient of the proton in the active materials, δ the thickness of the diffusion layer (the thickness of the active materials), c_{OH} the hydroxide concentration in the solution. When we balance the concentration on c_{Hm}, Eqs. 12 and 13 are obtained.

$$r_{1a} = r_{1c} + r_d \quad (12)$$

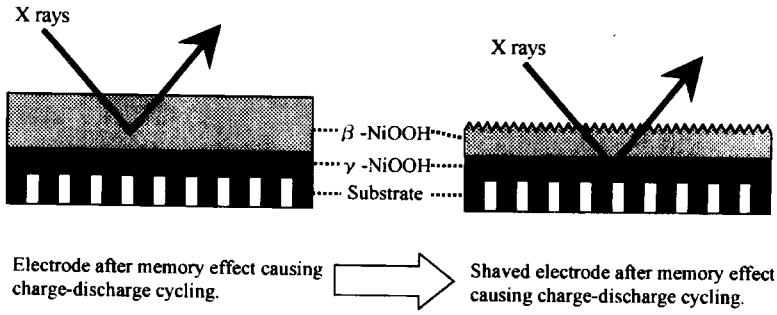

Fig. 19. X-Ray analysis image for γ-NiOOH formed on substrate.

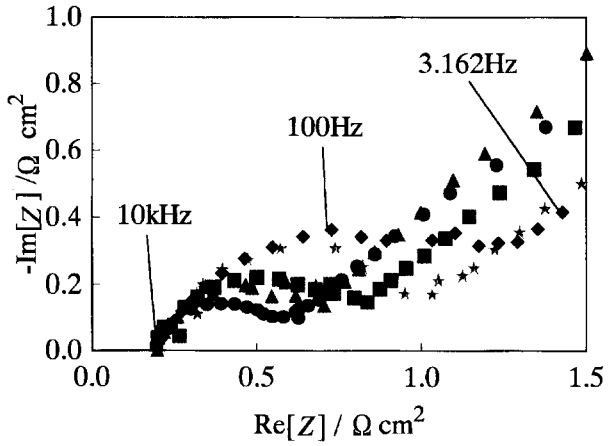

Fig. 20. Impedance spectra of charged-state Ni-electrode. ●: Electrode after normal charge–discharge cycling, ▲: electrode after 5 cycles memory effect causing charge–discharge cycling, ■: electrode after 10 cycles memory effect causing charge–discharge cycling, ⋆: electrode after 15 cycles memory effect causing charge–discharge cycling, ◆: electrode after 20 cycles memory effect causing charge–discharge cycling. Memory effect causing charge–discharge cycling was carried out at 3.2 mA cm^{-2} charging current for 6 h and at 3.2 mA cm^{-2} discharging current to an 0.8 V cutoff voltage.

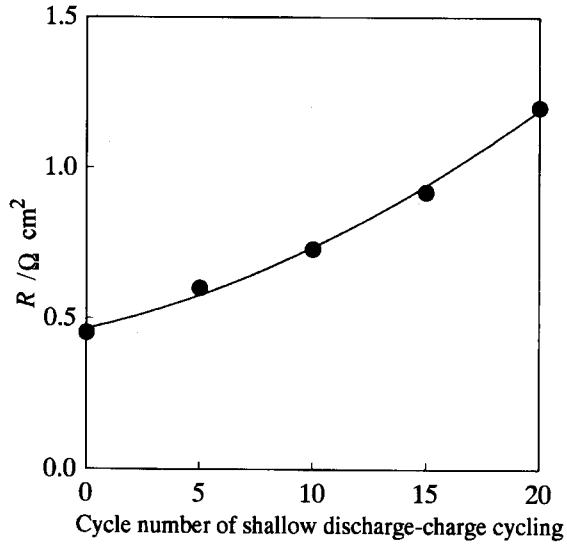

Fig. 21. Change in resistance value with cycle number of shallow discharge–charge cycling. Shallow discharge–charge cycling conditions are the same as in Fig. 20.

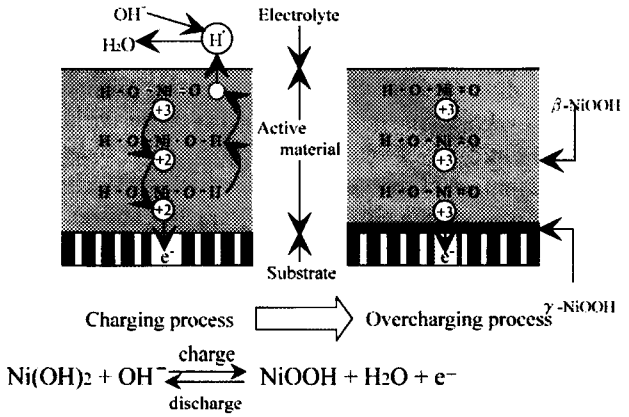

Fig. 22. Charging mechanism of Ni-electrode.

$$k_{1a}\theta = k_{1c}(1-\theta)c_{Hm} + \frac{D}{\delta}(c_{Hm} - c_{Hs}) \tag{13}$$

Similarly for the c_{Hs}, the following equations are obtained.

$$r_d + r_{hc} = r_{ha} \tag{14}$$

$$\frac{D}{\delta}(c_{Hm} - c_{Hs}) + k_{hc} = k_{ha}c_{Hs}c_{OH} \tag{15}$$

For the $[\{Ni(OH)_2\}_{ads}]$, Eqs. 16 and 17 hold.

$$r_{1c} + r_{er} = r_{1a} + r_{eb} \tag{16}$$

$$k_{1c}(1-\theta)c_{Hm} + k_{ef}(1-\theta)c_{NH} = k_{1a}\theta + k_{eb}\theta c_{NO} \tag{17}$$

From Eqs. 13, 15, and 17, two pairs of solutions are obtained for c_{Hm}, c_{Hs}, and θ as Eqs. 18, 20, and 22 and Eqs. 19, 21, and 23.

$$c_{Hm+} = \frac{P_1 + \sqrt{P_2}}{P_3} \tag{18}$$

$$c_{Hm-} = \frac{P_1 - \sqrt{P_2}}{P_3} \tag{19}$$

$$c_{Hs+} = \frac{\left(\frac{D}{\delta}c_{Hm+} + k_{hc}\right)}{\left(k_{ha}c_{OH} + \frac{D}{\delta}\right)} \tag{20}$$

$$c_{Hs-} = \frac{\left(\frac{D}{\delta}c_{Hm-} + k_{hc}\right)}{\left(k_{ha}c_{OH} + \frac{D}{\delta}\right)} \tag{21}$$

$$\theta_+ = \frac{\left\{k_{1c}c_{Hm} + \frac{D}{\delta}(c_{Hm+} - c_{Hs+})\right\}}{k_{1a} + k_{1c}c_{Hm+}} \tag{22}$$

$$\theta_{-} = \frac{\left\{k_{1c}c_{Hm} + \frac{D}{\delta}(c_{Hm-} - c_{Hs-})\right\}}{k_{1a} + k_{1c}c_{Hm-}} \tag{23}$$

In Eqs. 18 and 19, P_1, P_2, and P_3 are expressed as follows;

$$P_1 = -c_{NO}c_{OH}k_{1c}k_{eb}k_{ha} - \frac{D}{\delta}\{c_{OH}k_{1a}k_{ha} + c_{NH}c_{OH}k_{ef}k_{ha} + c_{NO}k_{eb}(k_{1c} + c_{OH}k_{ha}) - k_{1c}k_{hc}\} \tag{24}$$

$$P_2 = [c_{OH}k_{1c}(c_{NO}k_{eb} + 2c_{NH}k_{ef})k_{ha} + \frac{D}{\delta}\{2c_{NH}k_{1c}k_{ef} + c_{OH}k_{1a}k_{ha} + c_{NH}c_{OH}k_{ef}k_{ha} + c_{NO}k_{eb}(k_{1c} + c_{OH}k_{ha}) + k_{1c}k_{hc}\}]^2 - 4k_{1c}(c_{NO}k_{eb} + c_{NH}k_{ef})(\frac{D}{\delta} + c_{OH}k_{ha})(c_{NH}c_{OH}k_{1c}k_{ef}k_{ha}) + \frac{D}{\delta}\{c_{NH}k_{ef}(k_{1c} + c_{OH}k_{ha}) + k_{1c}k_{ha}\} \tag{25}$$

$$P_3 = 2\frac{D}{\delta}c_{OH}k_{1c}k_{ha} \tag{26}$$

Hereafter Eqs. 18, 20, and 22 are used because Eqs. 19, 21, and 23 give negative values. Regarding Eq. 1, rate constants k_{1a} and k_{1c} can be expressed as follows;

$$k_{1a} = (k_{1a})_0 \exp\{b_{1a}(E - E_1^\circ)\} \tag{27}$$

$$k_{1c} = (k_{1c})_0 \exp\{-b_{1c}(E - E_1^\circ)\} \tag{28}$$

where $(k_{1a})_0$ and $(k_{1c})_0$ are the anodic and cathodic rate constants at equilibrium potential E_1° respectively, E is the a. c. impedance measured potential, and b_{1a} ($= \alpha nF/RT$) and b_{1c} ($=(1-\alpha)nF/RT$) are the Tafel constants for the anodic and cathodic reactions. The steady-state current is expressed as Eq. 29.

$$I = F(r_{1a} - r_{1c}) = F\{k_{1a}\theta - k_{1c}(1 - \theta)c_{Hm}\} \tag{29}$$

The transient current resulting from both charge transfer and electrical double-layer charging is expressed as

$$I^t = F\{k_{1a}^t\theta^t - k_{1c}^t(1 - \theta^t)c_{Hm}^t\} + C_d\frac{dE^t}{dt} \tag{30}$$

where C_d denotes the double layer capacity at the electrode-solution interface. Subscript "t" represents the transient value. Using Eq. 27, k_{1a}^t is expressed as

$$\begin{aligned} k_{1a}^t &= (k_{1a})^\circ \exp\{b_{1a}(E + \Delta E - E_1^\circ)\} \\ &= (k_{1a})^\circ \exp\{b_{1a}(E - E_1^\circ) + b_{1a}\Delta E\} \\ &= (k_{1a})^\circ \exp\{b_{1a}(E - E_1^\circ)\}\exp(b_{1a}\Delta E) \\ &= k_{1a}\exp(b_{1a}\Delta E) \end{aligned} \tag{31}$$

By Taylor expansion of the index term in Eq. 31, the following Eq. 32 is obtained.

$$k_{1a}^t \approx k_{1a}(1 + b_{1a}\Delta E) \tag{32}$$

Similarly k_{1c}^t is expressed as

$$k_{1c}^t \approx k_{1c}(1 + b_{1c}\Delta E) \tag{33}$$

Combination of Eqs. 30, 32, and 33 yields the following expression.

$$I^t = I + \Delta I \approx F\{k_{1a}(1 + b_{1a}\Delta E)(\theta + \Delta\theta) - k_{1c}(1 - b_{1c}\Delta E)(1 - \theta - \Delta\theta)(c_{Hm} + \Delta c_{Hm})\} + C_d j\omega(E + \Delta E) \tag{34}$$

where ΔI is expressed as

$$\Delta I \approx F\{k_{1a}b_{1a}\Delta E\theta + k_{1a}\Delta\theta + k_{1c}b_{1c}\Delta E(1 - \theta)c_{Hm} - k_{1c}(1 - \theta)\Delta c_{Hm} + k_{1c}\Delta\theta c_{Hm}\} + C_d j\omega\Delta E \tag{35}$$

From Eq. 35, the reciprocal of the impedance Z_{rc} is given by the following Eq. 36,

$$\frac{1}{Z_{rc}} = \frac{\Delta I}{\Delta E} = F\left\{k_{1a}b_{1a}\theta + k_{1c}b_{1c}(1 - \theta)c_{Hm} + (k_{1a} + k_{1c}c_{Hm})\frac{\Delta\theta}{\Delta E} - k_{1c}(1 - \theta)\frac{\Delta c_{Hm}}{\Delta E}\right\} + C_d j\omega \tag{36}$$

This impedance Z_{rc} contains all processes such as electron transfer, adsorption–desorption, and diffusion processes. The impedance for each process, i.e., the electron transfer impedance Z_{rf}, the impedance containing electron transfer and adsorption–desorption process Z_{ra} and the impedance containing electron transfer and diffusion process Z_{rd} can be expressed as Eqs. 37, 38, and 39 respectively.

$$\frac{1}{Z_{rf}} = \frac{\Delta I}{\Delta E} = F\{k_{1a}b_{1a}\theta + k_{1c}b_{1c}(1 - \theta)c_{Hm}\} + C_d j\omega \tag{37}$$

$$\frac{1}{Z_{ra}} = \frac{\Delta I}{\Delta E} = F\left\{k_{1a}b_{1a}\theta + k_{1c}b_{1c}(1 - \theta)c_{Hm} + (k_{1a} + k_{1c}c_{Hm})\frac{\Delta\theta}{\Delta E}\right\} + C_d j\omega \tag{38}$$

$$\frac{1}{Z_{rd}} = \frac{\Delta I}{\Delta E} = F\left\{k_{1a}b_{1a}\theta + k_{1c}b_{1c}(1 - \theta)c_{Hm} - k_{1c}(1 - \theta)\frac{\Delta c_{Hm}}{\Delta E}\right\} + C_d j\omega \tag{39}$$

Here, the balance for change in the adsorbed nickel hydroxide [$\{Ni(OH)_2\}_{ads}$] by a small potential fluctuation is expressed as

$$\beta\frac{d\theta^t}{dt} = k_{1c}^t(1 - \theta^t)c_{Hm}^t + k_{ef}(1 - \theta^t)c_{NH} - k_{1a}^t\theta^t - k_{eb}\theta^t c_{NO} \tag{40}$$

where β is the molar concentration of adsorbed hydroxide per 1 cm^2 of collector. Inserting k_{1a}^t expressed as Eq. 32 and k_{1c}^t expressed as Eq. 33 into Eq. 40, one obtains Eq. 41:

$$\beta j\omega(\theta + \Delta\theta) \approx k_{1c}(1 - b_{1c}\Delta E)(1 - \theta - \Delta\theta)(c_{Hm} + \Delta c_{Hm}) + k_{ef}c_{NH}(1 - \theta - \Delta\theta) - k_{1a}(1 + b_{1a}\Delta E)(\theta + \Delta\theta) - k_{eb}c_{NO}(\theta + \Delta\theta) \tag{41}$$

The differential of Eq. 41 is expressed as Eq. 42.

$$\beta j\omega\Delta\theta \approx -k_{1c}b_{1c}\Delta E(1 - \theta)c_{Hm} + k_{1c}(1 - \theta)\Delta c_{Hm} - k_{1c}\Delta\theta c_{Hm} - k_{ef}c_{NH}\Delta\theta - k_{1a}b_{1a}\Delta E\theta - k_{1a}\Delta\theta - k_{eb}c_{NO}\Delta\theta \tag{42}$$

This Eq. 42 can be changed into the following Eq. 43:

$$\frac{\Delta\theta}{\Delta E} \approx \frac{-k_{1c}b_{1c}(1 - \theta)c_{Hm} - k_{1a}b_{1a}\theta + k_{1c}(1 - \theta)\frac{\Delta c_{Hm}}{\Delta E}}{\beta j\omega + k_{1c}c_{Hm} + k_{ef}c_{NH} + k_{1a} + k_{eb}c_{NO}} \tag{43}$$

The proton diffusion rate diffusing from the collector is expressed as

$$D\frac{\partial c^{t}_{Hm}}{\partial x}|_{x=o} = k^{t}_{1c}(1-\theta^{t})c_{Hm} - k^{t}_{1a}\theta^{t} \quad (44)$$

Inserting k^{t}_{1a} expressed as Eq. 32 and k^{t}_{1c} expressed as Eq. 33 into Eq. 44, one obtains the following equation:

$$D\frac{\partial(c_{Hm}+\Delta c_{Hm})}{\partial x}|_{x=o} = k_{1c}(1-b_{1c}\Delta E)(1-\theta-\Delta\theta)(c_{Hm}+\Delta c_{Hm}) - k_{1a}(1+b_{1a}\Delta E)(\theta+\Delta\theta) \quad (45)$$

Also, the following equation holds:

$$D\frac{\partial \Delta c_{Hm}}{\partial x}|_{x=o} = -k_{1c}b_{1c}\Delta E(1-\theta)c_{Hm} + k_{1c}(1-\theta)\Delta c_{Hm} - k_{1c}c_{Hm}\Delta\theta - k_{1a}b_{1a}\Delta E\theta - k_{1a}\Delta\theta \quad (46)$$

Substituting $y = x/\delta \Leftrightarrow x = \delta y$ into above Eq. 44, one obtains the following Eq. 47:

$$\frac{D}{\delta}\frac{\partial \Delta c_{Hm}}{\partial y}|_{y=o} = -k_{1c}b_{1c}\Delta E(1-\theta)c_{Hm} - k_{1a}b_{1a}\Delta E\theta + k_{1c}(1-\theta)\Delta c_{Hm} - (k_{1c}c_{Hm}+k_{1a})\Delta\theta \quad (47)$$

By the way, Warburg impedance is expressed as Eq. 48.[29]

$$W = \frac{\tanh\left(\delta\sqrt{\frac{j\omega}{D}}\right)}{\sqrt{j\omega D}} = \frac{-\Delta c_{Hm}}{\frac{D}{\delta}\frac{\partial \Delta c_{Hm}}{\partial y}\Big|_{y=o}} \quad (48)$$

Combining Eqs. 47 and 48 yields the following equation:

$$-\frac{\Delta c_{Hm}}{W} = -k_{1c}b_{1c}\Delta E(1-\theta)c_{Hm} - k_{1a}b_{1a}\Delta E\theta + k_{1c}(1-\theta)\Delta c_{Hm} - (k_{1c}c_{Hm}+k_{1a})\Delta\theta \quad (49)$$

If one changes Eq. 49, the following equation is obtained:

$$\frac{\Delta c_{Hm}}{\Delta E} = \frac{k_{1c}b_{1c}(1-\theta)c_{Hm} + k_{1a}b_{1a}\theta + (k_{1c}c_{Hm}+k_{1a})\frac{\Delta\theta}{\Delta E}}{k_{1c}(1-\theta)+\frac{1}{W}} \quad (50)$$

Now, we can obtain the impedance corresponding to each process by introducing $\Delta\theta/\Delta E$ and $\Delta c_{Hm}/\Delta E$ expressed as Eqs. 43 and 50 into Eqs. 36, 37, 38, and 39, respectively.

A schematic illustration of the Nyquist plot for the complex impedance spectrum described by Eqs. 36, 37, 38, and 39 is given in Fig. 23, where the solution resistance (R_{sol}) is added to the real part of each process. From this Fig. 23, it is found that the impedance loop in the high frequency region corresponds to electron transfer and adsorption–desorption processes and the linear part in the low frequency region corresponds to the diffusion process. Parameters used in calculation are adjusted to be fitted to the experimental loop. However, curve-fitting using Eq. 36 did not give a good result as shown in Fig. 24, where the calculated curve is the same as Fig. 23(A). Therefore, another impedance due to charge-transfer corresponding to Eq. 2′ was considered. The equivalent circuit is shown in Fig. 25, and the corresponding impedance is expressed as Eq. 51.

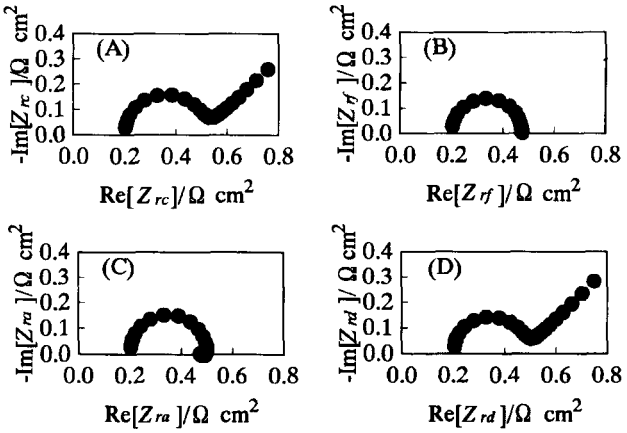

Fig. 23. Calculated impedance diagrams including various processes. (A) Impedance including charge-transfer, adsorption-desorption and diffusion processes, (B) impedance including charge-transfer process, (C) impedance including charge-transfer and adsorption–desorption processes, (D) impedance including charge-transfer and diffusion processes. Parameters are as follows: $C_d = 6\times10^{-4}$ F cm^{-2}, $R_{sol} = 0.2$ Ω cm^2, $E = 0.43$ V, $\beta = 10^{-5}$ mol cm^{-2}, $(k_{1a})_0 = 10^{-5}$ mol cm^{-2} s^{-1}, $(k_{1c})_0 = 10^{-3}$ cm s^{-1}, $k_{ef} = 10^{-3}$ cm s^{-1}, $k_{eb} = 10^{-3}$ cm s^{-1}, $k_{ha} = 0.1$ mol^{-1} cm^4 s^{-1}, $k_{hc} = 10^{-6}$ mol cm^{-2} s^{-1}, $b_{1a} = 19$ V^{-1}, $b_{1c} = 19$ V^{-1}, $E^{\circ}_1 = 0.43$ V, $c_{NH} = 0.01$ mol cm^{-3}, $c_{NO} = 0.09$ mol cm^{-3}, $c_{OH} = 8\times10^{-3}$ mol cm^{-3}, $D = 5\times10^{-8}$ cm^2 s^{-1}, $\delta = 0.025$ cm.

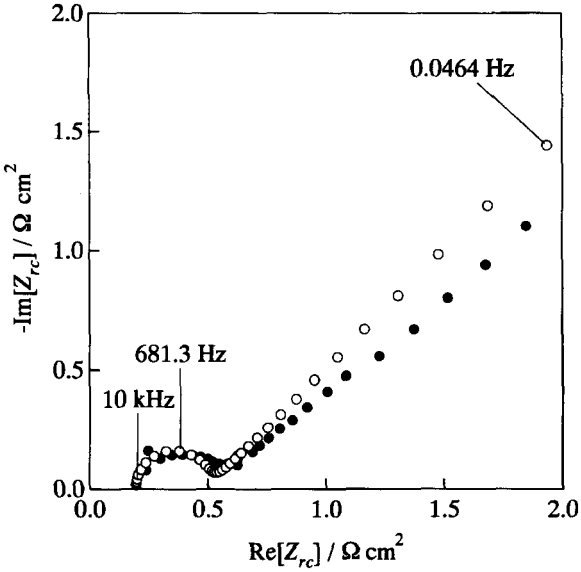

Fig. 24. Experimental (●) and calculated (○) impedance diagrams. ●: impedance of charged state Ni-electrode after normal charge-discharge cycling, ○: impedance calculated from Eq. 36; parameters are the same as those in Fig. 23.

$$Z_{rce} = R_{sol} + Z_{rc} + \frac{1}{C_e j\omega + \frac{1}{R_e}} \quad (51)$$

Using this equation, curve-fitting for the charged state of a normal Ni-electrode was carried out. Both measured and calculated impedances agree rather well as shown in Fig. 26. In the measured impedance of charged-state, a loop observed

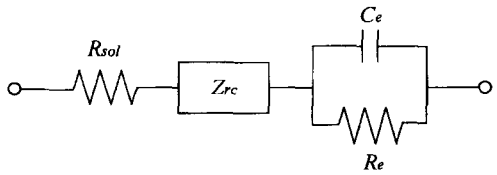

Fig. 25. Equivalent circuit for Ni-electrode. R_{sol} : Solution resistance, Z_{rc} : impedance of charge-transfer, adsorption–desorption and proton-diffusion processes, R_e : electron-transfer resistance, C_e : electron-transfer capacitance.

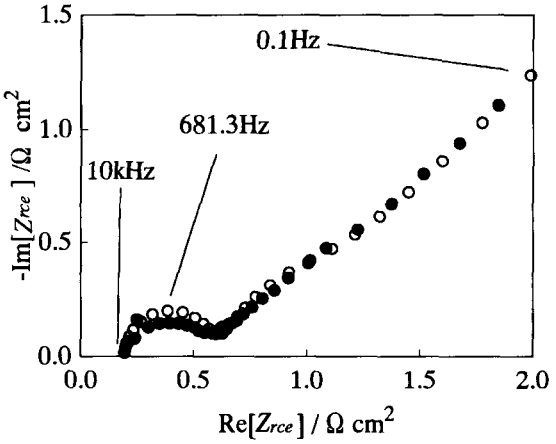

Fig. 26. Comparison of measured and calculated impedance. ●: Impedance of charged state Ni-electrode after normal charge–discharge cycling, ○: impedance calculated using Eq. 51. Parameters are the same as those in Fig. 23 except $(k_{1a})_0 = 8\times10^{-6}$ mol cm^{-2} s^{-1}, $C_e = 0.4$ F cm^{-2}, and R_e = 0.2 Ω cm^2.

in the high frequency region is slightly distorted compared to that of the calculated one, because the double layer capacitor of the Ni-electrode is not an ideal condenser. This phenomenon is often observed in an electrode with a rough electrode surface.[30—32]

Because γ-NiOOH is known to be hard to discharge,[33] we replaced this phenomenon with small values of $(k_{1a})_0$ and $(k_{1c})_0$ in Eqs. 27 and 28. Figure 27 shows the calculated impedance loops changing only with $(k_{1a})_0$ and $(k_{1c})_0$ in Eq. 51 and using other parameters in Fig. 26. As seen in this Fig. 27, the impedance loops become large as rate constants $(k_{1a})_0$ and $(k_{1c})_0$ become small. Namely, the quantity of γ-NiOOH at the interface between the collector and the active materials is considered to increase as shallow discharge–charge cycling progresses, and the charge transfer resistance increases, which enlarges the impedance loop observed at the high frequency side in Fig. 20.

4. Conclusions

From all these results and discussion, we concluded that

1. The main cause of the memory effect observed in alkaline-type rechargeable batteries using a nickel electrode is the formation of γ-NiOOH.

2. γ-NiOOH initially forms at the collector side and grows to the solution side as shallow discharge–charge cycling progresses. Therefore, if the amount of formed γ-NiOOH is small, X-rays cannot reach the γ-NiOOH phase and only β-NiOOH can be detected in XRD analysis. We think this is the reason why γ-NiOOH cannot be detected on a nickel electrode even when a memory effect is observed.

3. Once γ-NiOOH is formed at the collector side, it may increase the charge transfer resistance, which lowers the working potential on the charging process, i.e., a memory effect appears.

4. This γ-NiOOH disappears within a few cycles of normal charge–discharge cycling.

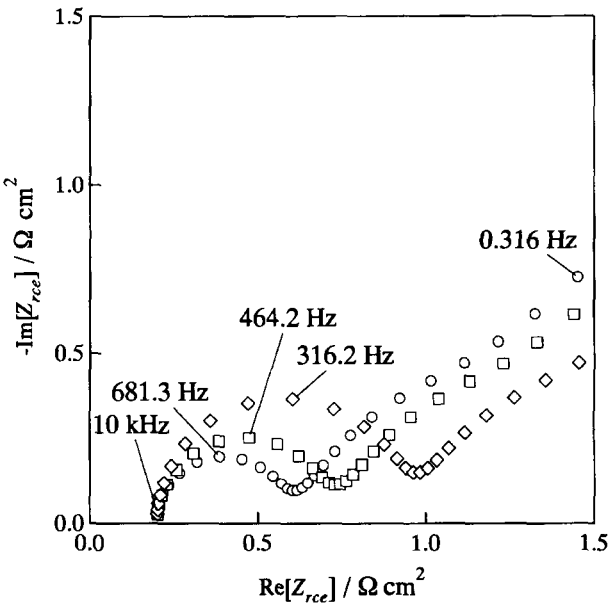

Fig. 27. Change of impedance with $(k_{1a})_0$ and $(k_{1c})_0$. Parameters are the same as those in Fig. 26 except $(k_{1a})_0$ and $(k_{1c})_0$. ○: $(k_{1a})_0 = 8\times10^{-6}$ mol cm^{-2} s^{-1}, $(k_{1c})_0 = 10^{-3}$ cm s^{-1}, □: $(k_{1a})_0 = 6\times10^{-6}$ mol cm^{-2} s^{-1}, $(k_{1c})_0 = 7.5\times10^{-4}$ cm s^{-1}, ◇: $(k_{1a})_0 = 4\times10^{-6}$ mol cm^{-2} s^{-1}, $(k_{1c})_0 = 5\times10^{-4}$ cm s^{-1}.

The authors express their thanks for a Grant-in-Aid for Scientific Research No. 10650817 from the Ministry of Education, Science, Sports and Culture.

References

1 C. Lurie, "Extended Abstract of 15th Intersociety Energy Conversion Engineering Conference," Abstr., p. 1634 (1980).

2 T. R. Crompton, "Battery Reference Book," Sect. 19.1.2, Butterworths, London (1990).

3 S. Venkatesan, M. Fetcenko, B. Reichman, D. Magnuson, and S. K. Dhar, "Proceedings of the 33rd International Power Sources Symposium," Cherry Hill, NJ, June13—16, 1988, The Electrochemical Society Inc., Abstr., p. 476 (1988).

4 X. Xia and Z. Guo, *J. Electrochem. Soc.*, **144**, L213 (1997).

5 K. Takeno, K. Ikeda, N. Shiojima, H. Hasebe, and Y. Sato, "31st Battery Symposium," Japan, Abstr., p. 157 (1990).

6 N. Sato, K. Yagi, and T. Sakurai, "EVS-15 Proceedings," Brussels, October, 1998, Abstr., p. 1.

7 S. Kuwajima, K. Nakatani, and K. Takagi, "34th Battery Symposium," Japan, Abstr., p. 253 (1993).

8 Y. Sato, K. Ito, T. Arakawa, and K. Kobayakawa, *J. Electrochem. Soc.*, **143**, L225 (1996).

9 E. J. Rubbing and B. Baboon, *J. Electrochem. Soc.*, **118**, 428 (1971).
10 I. Matsumoto, M. Ikeyama, T. Iwaki, and H. Ogawa, *Denki Kagaku*, **54**, 159 (1986).
11 B. B. Ezhof and O. G. Malandin, *J. Electrochem. Soc.*, **138**, 885 (1991).
12 W. -H. Zhu, J. -J. Ke, H. -M. Yu, and D. -J. Zhang, *J. Power Sources*, **56**, 75 (1995).
13 P. Oliva, J. Leonardi, J. F. Laurent, C. Delmas, J. J. Braconnier, M. Figlarz, F. Fievet, and A. de Gulbert, *J. Power Sources*, **8**, 229 (1981).
14 N. Yu. Uflyand and S. A. Rozentsveig, "Sbornik Rabot po Khimicheskim Istochnikam Toka," Energiya, Leningrad (1986), Abstr., p. 180, No. 3.
15 R. Barnard, C. F. Randel, and F. L. Tye , *J. Electroanal. Chem.*, **119**, 17 (1981).
16 H. Bode, K. Dehmelt, and J. Witte, *Z. Anorg. Chem.*, **366**, 1 (1969).
17 Discussion at the 37th Battery Symposium, Japan (1996).
18 N. Sac- Epée, M. R. Palacìn, B. Beaudoin, A. Delahaye-Vidal, T. Jamin, Y. Chabre, and J-M. Tarâscon, *J. Electrochem. Soc.*, **144**, 3896 (1997).
19 N. Sac-Epée, M. R. Palacìn, A. Delahaye-Vidal, Y. Chabre, and J-M. Tarâscon, *J. Electrochem. Soc.*, **145**, 1434 (1998).
20 C. Léger, C. Tessier, M. Ménétrier, C. Denage, and C. Delmas, *J. Electrochem. Soc.*, **146**, 924 (1999).
21 I. Matsumoto, M. Ikeyama, T. Iwaki, and H. Ogawa, *Denki Kagaku*, **54**, 159 (1986).
22 B. B. Ezhov and O. G. Malandin, *J. Electrochem. Soc.*, **138**, 885 (1991).
23 Wen-Hua Zhu, Jia-Jun Ke, Hong-Mei Yu, and Deng-Jun Zhang, *J. Power Sources*, **56**, 75 (1995).
24 Z. Chang, H. Tang, and J. G. Chen, *Electrochem. Commun.*, **1**, 513 (1999).
25 C. D. H. Bradhurst, S. X. Dou, and H. K. Liu, *J. Electrochem. Soc.*, **146**, 3606 (1999).
26 Y. Sato, S. Takeuchi, and K. Kobayakawa, *J. Power Sources*, accepted.
27 K. H. J. Bushow, P. C. P. Bouten, and A. R. Miedema, *Rep. Prog. Phys.*, **45**, 937 (1982).
28 S. Tkeuchi, S. Magaino, K. Kobayakawa, and Y. Sato, *Electrochemistry*, **68**, No. 12 (2000), to be published.
29 M. Matlosz., S. Magaino, and D. Landolt, *J. Electrochem. Soc.*, **141**, 410 (1994).
30 P. Ferloni, M. Mastragostino, and L. Meneghello, *Electrochim. Acta*, **41**, 27 (1996).
31 S.-I. Pyun and J.-S. Bae, *Electrochim. Acta*, **41**, 919 (1996).
32 T. Piao, S.-M. Park, C.-H. Doh, and S.-1. Moon, *J. Electrochem. Soc.*, **146**, 2794 (1999).
33 N. Sac-Epée, M. R. Palacìn, and A. Delahaye-Vidal, *J. Electrochem. Soc.*, **145**, 1434 (1998).

Yuichi Sato was born in Nagaoka, Niigata, in 1939. He graduated from Department of Chemistry, Faculty of Science, Tohoku University in 1962, and received his master's degree from the same university in 1964. He was appointed as a research assistant at the above department in 1962 and received his doctoral degree from Tohoku University in 1969. From 1969 to 1984, he worked at Research and Development Center, Toshiba Corporation and then transferred to Toshiba Battery Company. He was appointed as an associate professor at the Department of Applied Chemistry, Faculty of Engineering, Kanagawa University in 1987 and has been promoted to professor in 1993. His current research interests includes high-energy density battery materials and electro- and electroless plating. He received the progress award for young chemists from the Chemical Society of Japan in 1974 and the Tanahashi technical prize from the Electrochemical Society of Japan in 1984.

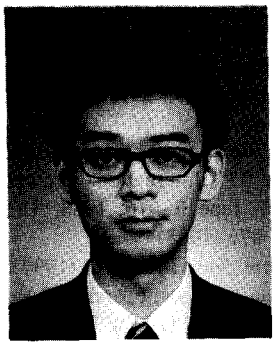

Shigeo Takeuchi was born in Yamanashi in 1975. He graduated from Department of Applied Chemistry, Faculty of Engineering, Kanagawa University in 1998, and graduated from Graduate School of Engineering, Kanagawa University in 2000. He is now working at Tomiyama Pure Chemical Industries Ltd..

Shin'ichi Magaino was born in Yokohama in 1950. He received his Ph. D. in 1988 at Waseda University under the direction of Professor Tetsuya Osaka for his work on the electrochemical measurements of metal corrosion. Since 1974, he has been working at Kanagawa Industrial Technology Research Institute. From 1991 to 1992 he worked with Professor Dieter Landolt at Swiss Federal Institute of Technology in Lausanne (EPFL) as a visiting scientist. His main research field is the electrochemical analysis of corrosion and batteries.

Koichi Kobayakawa was born in 1941 in Yokohama, Japan. He graduated from Kanagawa University in 1967 and obtained Dr. Engineering degree from the University of Tokyo in 1994. He was appointed as a technician of Kanagawa University in 1961 and research associate of the same University in 1970. His research interests cover photocatalyst, catalytic combustion, and electroless plating.